AI26 inhibits the ADP-ribosylhydrolase ARH3 and suppresses DNA damage repair

Xiuhua Liu, Rong Xie, Lily L. Yu, Shih-Hsun Chen, Xiaoyun Yang, Anup K. Singh, Hongzhi Li, Chen Wu and Xiaochun Yu

Supplemental Figure 1

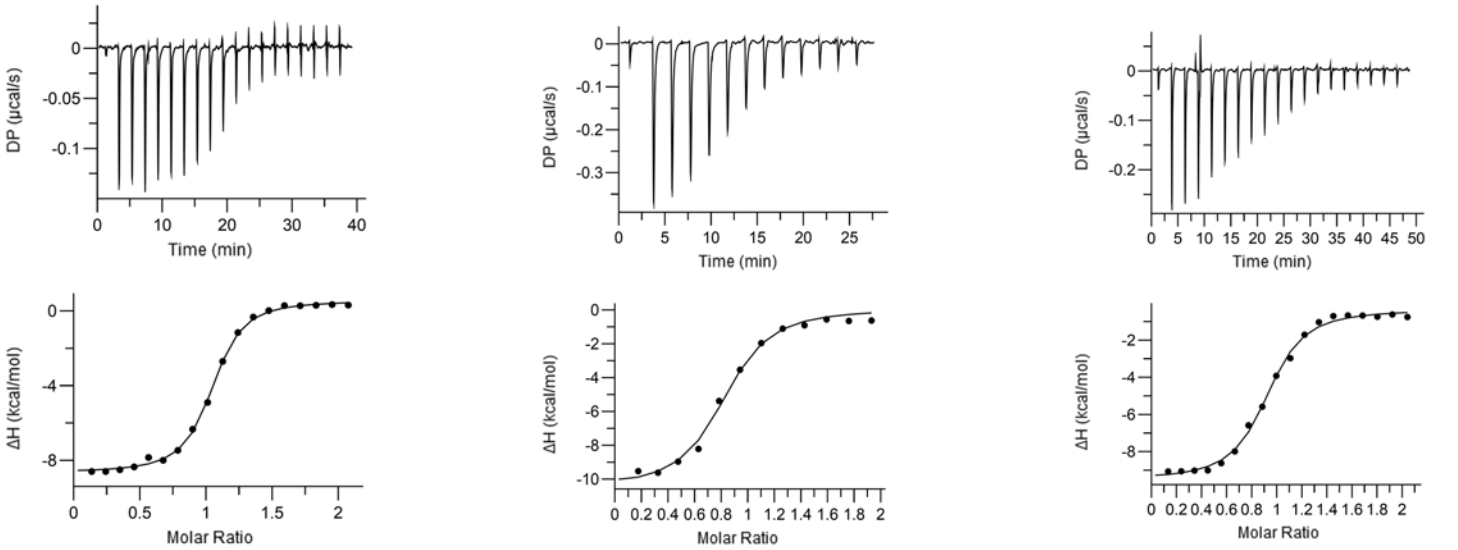

Kd = 2.16 ± 0.35 µM

Kd = 1.48 ± 0.26 µM

Kd = 1.82 ± 0.29 µM

Supplemental Figure 1. The binding affinity between AI26 and ARH3 is obtained from three independent ITC assays.

Supplemental Figure 2

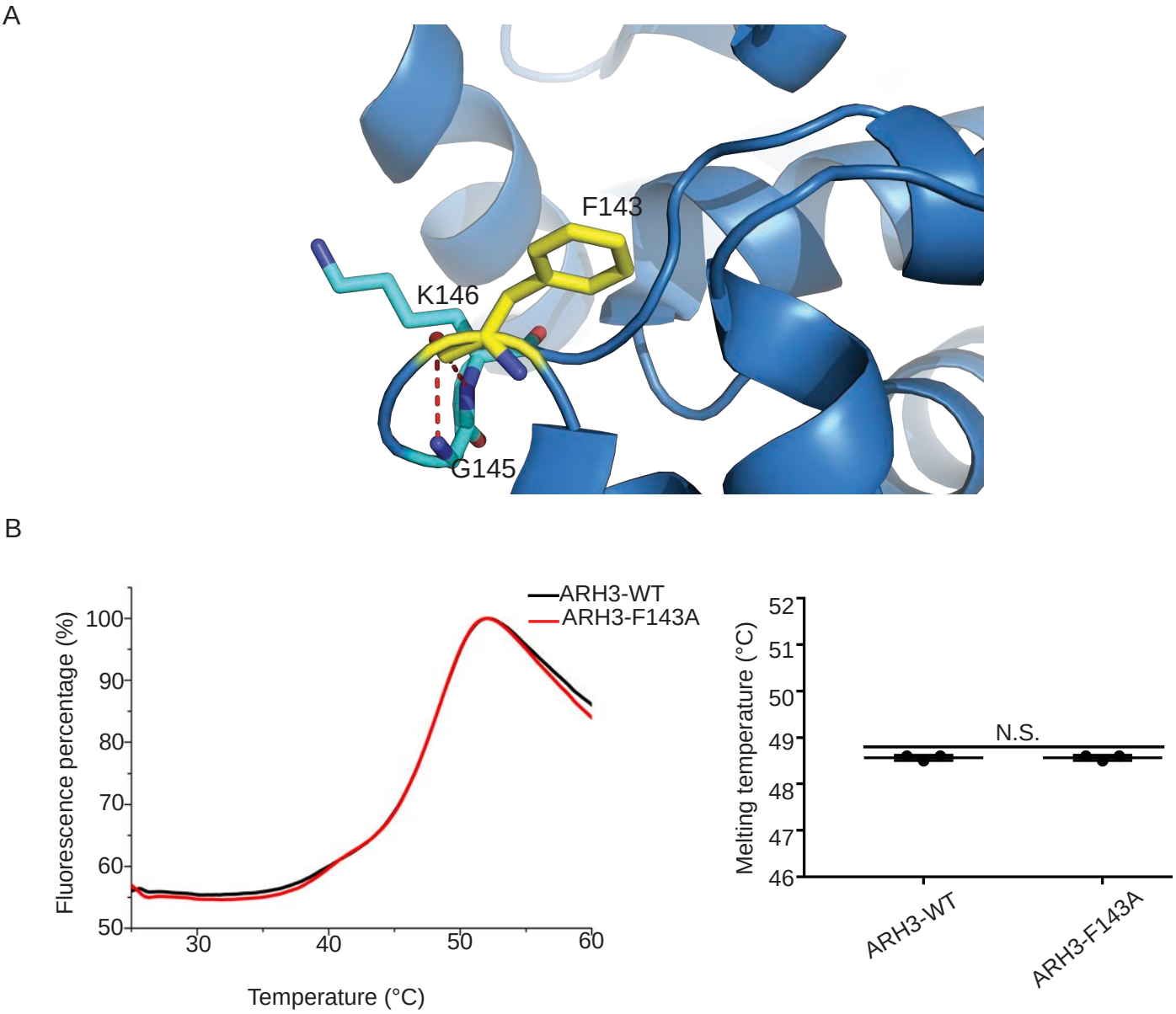

Supplemental Figure 2. The F143A mutant does not affect the overall folding of ARH3. (A) Structural analysis of Phe[143] in the overall folding of ARH3. The overall structure of ARH3 is in blue cartoon. Phe[143] is in yellow stick, and its interacting residues Gly[145] and Lys[146] are in cyan sticks. The hydrogen bonds are in red dashes. (B) The thermal shift analysis of wild type ARH3 and the F143A mutant. Three independent experiments were carried out. N.S.: non-significant.

Supplemental Figure 3

A

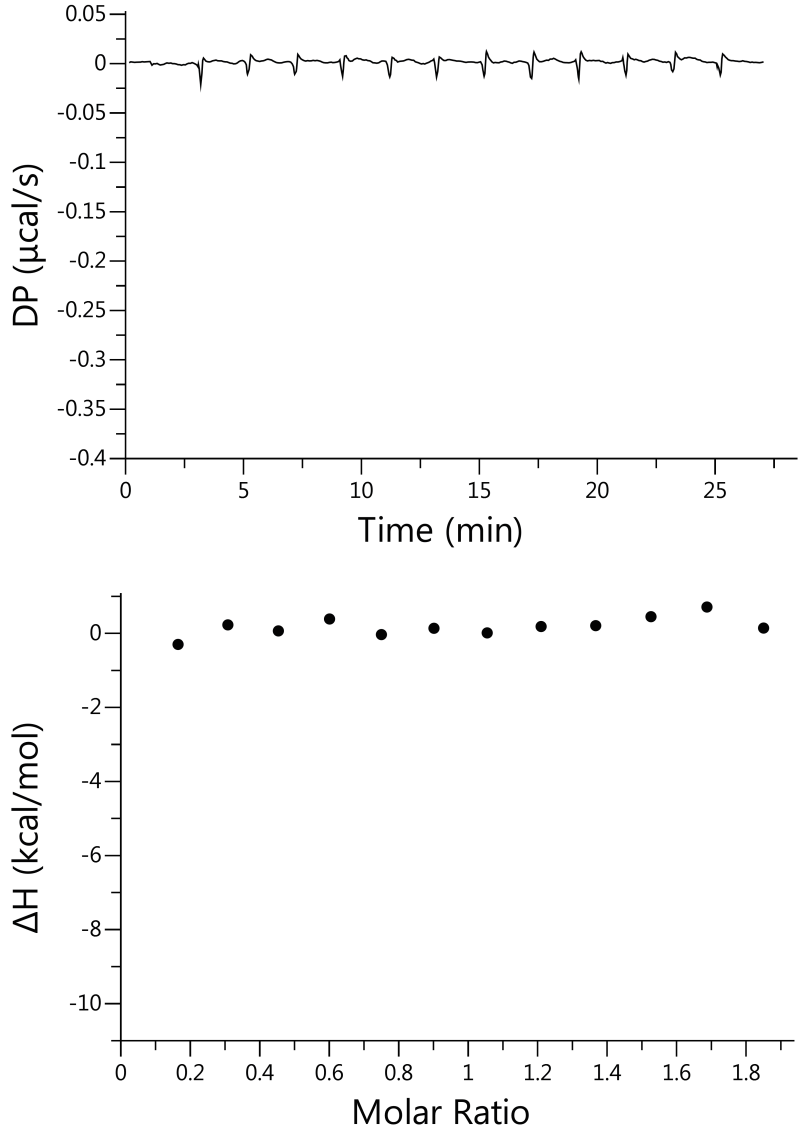

B

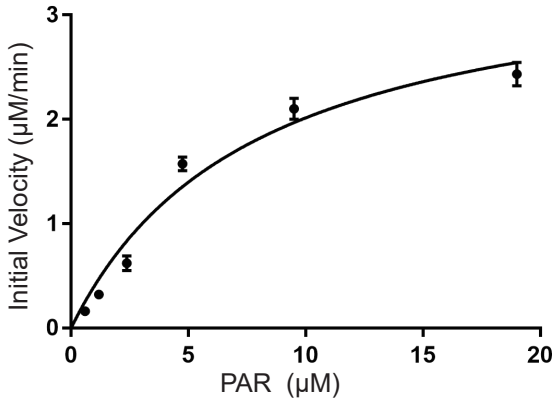

ARH3-wild type

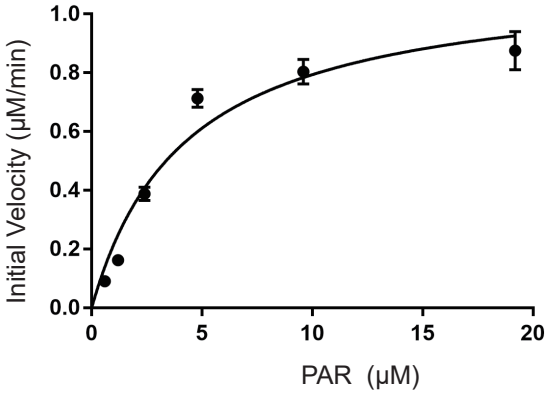

ARH3-F143A

The Michaelis-Menton kinetic parameters of ARH3 and its F143A mutant

Proteins	K_m (μM)	V_{max} (μM/min)	K_{cat} (s^{-1})	K_{cat}/K_m (M^{-1} s^{-1})
ARH3-wild type	7.87±1.43	3.60±0.29	0.6±0.04	7.62×10^4
ARH3-F143A	4.25±0.76	1.13±0.07	0.18±0.01	4.23×10^4

Supplemental Figure 3. Characterization of recombinant ARH3 and the F143A mutant. (A) Affinity between the F143A mutant and AI26 was examined by ITC**.** (B) Enzyme kinetics of wild type ARH3 and the F143A mutant were calculated by Michaelis-Menten equation. Initial rates were plotted against substrate concentration and fit to the Michaelis-Menten equation via a non-linear curve-fitting algorithm through GraphPad Prism 7 software. Three independent experiments were performed.

Supplemental Figure 4

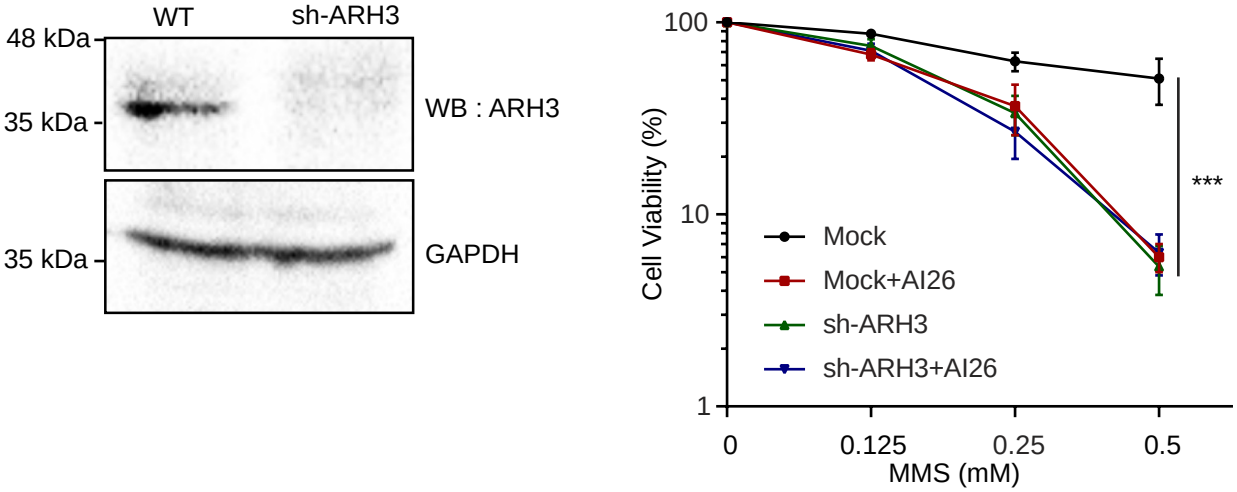

Supplemental Figure 4. ARH3-deficient cells are insensitive to AI26 treatment. Following the pre-treatment with AI26, both wild type U2OS and ARH3-deficient PEO1 cells were treated with the indicated concentration of MMS respectively, and then seeded at colony-forming density. Cells were stained using crystal violet after 14 days culture. Both wild type U2OS and ARH3-deficient cells only treated with MMS were used as controls. Cell viability is displayed as mean ± SD from three independent experiments. ***: statistically significant ($P < 0.001$).

Supplemental figure 5

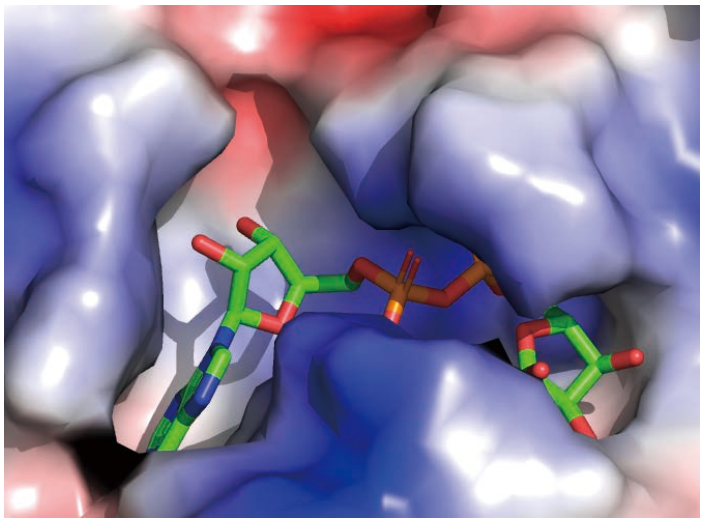

MacroD2

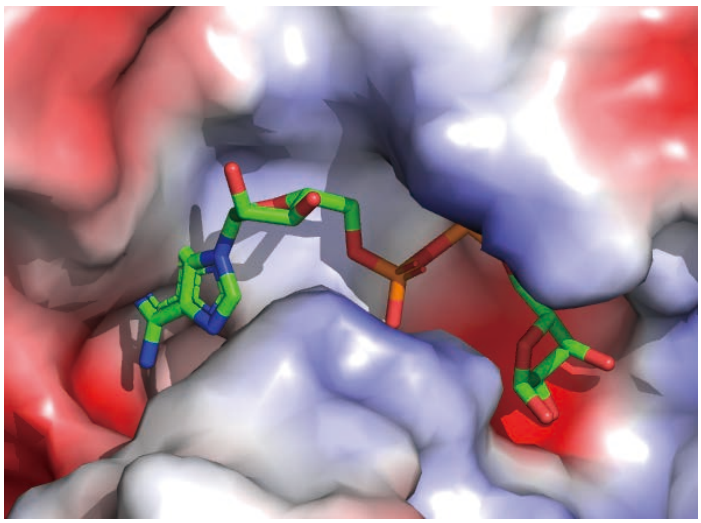

PARG

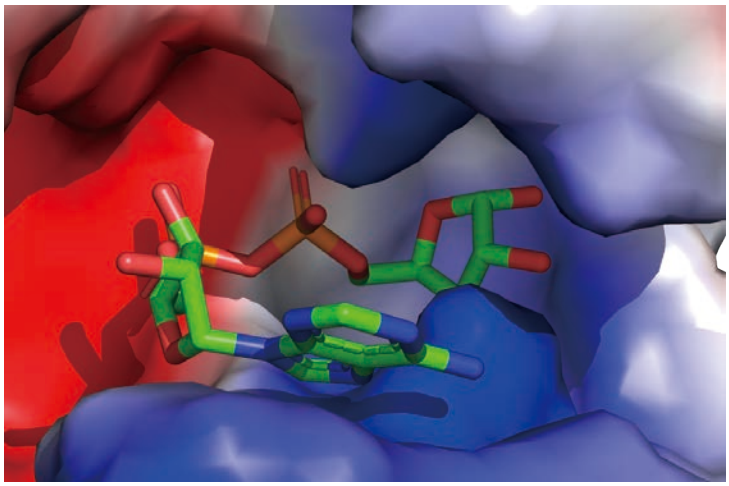

Nudt5

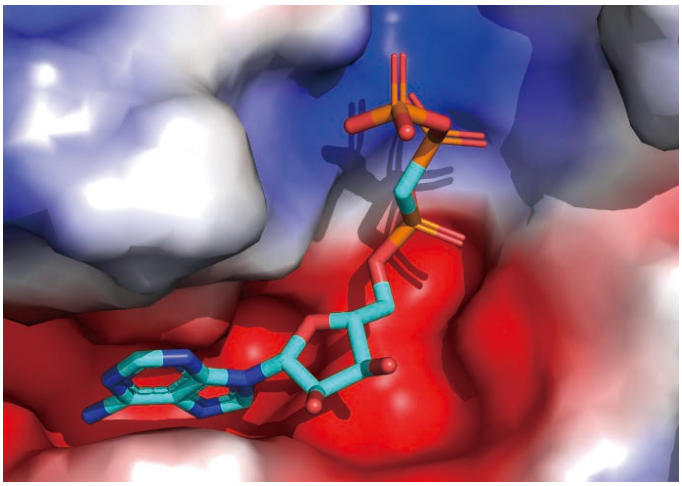

ENPP3

Supplemental Figure 5. The structural comparison of the catalytic pockets of the macro domain ADPR hydrolases and pyrophosphatases. The catalytic pockets are shown in electrostatic potential map, and the ADPR molecule is included in the catalytic pocket of human MacroD2 (pdb: 4IQY), Nudt5 (pdb: 2DSC) and PARG (pdb: 4B1H, 4A0D) respectively, and is shown in green stick. The ATP analog alpha, beta-methylene ATP was included in the catalytic site of human ENPP3 (pdb: 6C02), and is displayed in cyan stick.